

Effect of crystallographic orientation in textured $\text{Ba}_{0.92}\text{Ca}_{0.08}\text{TiO}_3$ piezoelectric ceramics

Astri Bjørnetun Haugen,¹ Maxim I. Morozov,¹ Mats Johnsson,² Tor Grande¹ and Mari-Ann Einarsrud¹

¹ Department of Materials Science and Engineering, Norwegian University of Science and Technology (NTNU), Trondheim, Norway

² Department of Materials and Environmental Chemistry, Stockholm University, Stockholm, Sweden

Abstract

Strongly textured lead-free $\text{Ba}_{0.92}\text{Ca}_{0.08}\text{TiO}_3$ piezoelectric ceramics were fabricated by tape casting and templated grain growth. Dense ceramics with both favorable $\langle 100 \rangle$ and unfavorable $\langle 111 \rangle$ texture were successfully prepared. Enhanced piezoelectric performance was demonstrated for ceramics with $\langle 100 \rangle$ texture, in line with the predictions based on reported piezoelectric coefficients of tetragonal BaTiO_3 . Due to the expanded tetragonal range through Ca-substitution, $\langle 100 \rangle$ texture is favorable over a wide temperature range. The $\langle 100 \rangle$ texture also results in the enhanced piezoelectric performance being temperature-independent. In addition to engineering of stable, high-performance lead-free piezoelectric ceramics, this study has demonstrated that consideration of the extender/rotator nature of piezoelectric properties are imperative for improving the piezoelectric response through texturing.

Introduction

Grain texture, which is a preferential alignment of grains and crystallographic axes,¹ has long been utilized to increase the piezoelectric response of piezoelectric ceramics.² However, the preferred crystallographic orientation of the texture is rarely justified and the mechanisms by which texturing improve the performance are not well understood.¹ Since the intrinsic piezoelectric effect is inherently anisotropic,³ both single crystals and textured ceramics are expected to display anisotropic intrinsic piezoelectric response. The crystallographic direction that exhibits the maximum response is however not intuitively known for a given material. For example, the total intrinsic longitudinal piezoelectric effect (d_{33}^*) in tetragonal perovskites, depends on the values of the piezoelectric coefficients d_{ij} and the angle between the electric field and the polar axes (θ) as expressed in Equation 1:^{4,5}

$$d_{33}^* = d_{31}(\cos\theta\sin^2\theta) + d_{15}(\cos\theta\sin^2\theta) + d_{33}\cos^3\theta \quad (1)$$

Since the piezoelectric coefficients depend on both the stoichiometry and the temperature, the direction of maximum response must be carefully assessed for each material. Based on the direction of maximum d_{33}^* from Equation 1, ferroelectrics can be classified either as “extenders”, which display the maximum response parallel to the polar axis, or “rotators”, where the maximum response is away from the polar axis.^{4,6} The crystallographic direction of maximum intrinsic response can therefore only be utilized when the rotator or extender nature of the material is known. Experiments on single crystals have confirmed the improved piezoelectric response along the same crystallographic directions as predicted by theory.⁷⁻¹¹

While the *intrinsic* piezoelectric contribution and the rotator/extender nature are equal for a single crystal and an ideally textured ceramic with the same composition, the *extrinsic* piezoelectric properties are not. Intergranular interactions, which are not present in single crystals, contribute significantly to the piezoelectric effect in polycrystals.¹² Textured ceramics further differ from ceramics with randomly oriented grains, since the alignment of the grains also results in an alignment of the ferroelastic strain. Such alignment allows cooperative domain reorientation that increases the poling efficiency,¹ providing an extrinsic path for improved piezoelectric response through texturing. Therefore, the origin of any improvement introduced by texturing cannot be readily assigned to either intrinsic or extrinsic mechanisms. Furthermore, it is possible that texturing in an intrinsically unfavorable direction (e.g. parallel to the polar axis in a rotator ferroelectric) still results in an overall improvement due to the extrinsic effect of aligned strains and improved poling. Contrary to single crystals, anisotropy of textured ceramics is not investigated to a great extent.

Texturing is a proven approach to narrow the performance gap between lead-free piezoelectrics and the $\text{Pb}(\text{Zr},\text{Ti})\text{O}_3$ (PZT)-based ceramics. One well-known example is the $(\text{K},\text{Na})\text{NbO}_3$ system, where the combination of texture and doping resulted in performance comparable to lead-based piezoelectrics.¹³ In this case, the improvement observed with $\langle 100 \rangle_{\text{pc}}$ texture can be ascribed to the rotator ferroelectricity of KNN.¹⁴ More recently, $\text{Ba}_{0.85}\text{Ca}_{0.15}\text{Zr}_{0.10}\text{Ti}_{0.90}\text{O}_3$ (BCZT) exhibited piezoelectric constants higher than soft PZT in *non-textured* ceramics.¹⁵ A modest improvement in the piezoelectric properties has been reported for $\langle 100 \rangle$ -textured compared to non-textured BCZT,¹⁶ yet the values for both textured and non-textured ceramics were lower than commonly reported values for non-textured BCZT.^{15,17,18} The high performance in this system is attributed to phase instability, either by thermal and compositional proximity to phase transitions,^{15,19} and/or tetragonal and rhombohedral phase coexistence at room temperature^{20,21}. These have significant ramifications: the phase coexistence masks the origin of the enhanced response (rotator or extender ferroelectricity), while phase instability causes both undesirable temperature-dependent properties and also affects the rotator/extender properties of BCZT. These issues can be largely avoided through a simplification of the stoichiometry to $(\text{Ba},\text{Ca})\text{TiO}_3$ which reduces the piezoelectric response,²² but improves the phase stability of the tetragonal phase.²³ This is because T_C increases slightly with x in $\text{Ba}_{1-x}\text{Ca}_x\text{TiO}_3$ until it peaks at ~ 130 °C for $x = 0.08$, while the $T_{\text{T-O}}$ decreases monotonically with x and is ~ -40 °C at $x = 0.08$.²³

In this work we investigate the effect of $\langle 100 \rangle$ and $\langle 111 \rangle$ texturing on the piezoelectric properties of $\text{Ba}_{0.92}\text{Ca}_{0.08}\text{TiO}_3$ (BCT) with the aim of engineering high-performance lead-free piezoceramics. The choice of BCT as the model material stems from its temperature-stable tetragonal phase and relatively high T_C , in contrast to the phase-instability and lower T_C of BCZT. We demonstrate how broadening of the stable temperature range of the tetragonal

phase can cause extender ferroelectricity over a wide temperature range, supported by observations of increased piezoelectric response with $\langle 100 \rangle$ texture (electric field parallel to the polar axis) and decreased response with $\langle 111 \rangle$ -texture (electric field parallel to a non-polar axis).

Experimental

BCT matrix powders were manufactured by solid state synthesis. CaCO_3 ($\geq 99.95\%$, Sigma-Aldrich, St Louis, MO, USA) was ball milled with yttria stabilized zirconia (YSZ) milling media in isopropanol for 36 h to reduce the particle size. Stoichiometric amounts of CaCO_3 , BaCO_3 ($\geq 99\%$, Sigma-Aldrich, St Louis, MO, USA) and TiO_2 (anatase) (99.8% , Sigma-Aldrich, St Louis, MO, USA) were mixed by ball milling with YSZ balls in isopropanol for 4 h. The mixture was calcined at $950\text{ }^\circ\text{C}$ for 8 h and then further ball milled for 8 h. Finally, the powder was sieved at $250\text{ }\mu\text{m}$.

(100)-oriented BaTiO_3 platelet templates were synthesized by molten salt synthesis and conversion based on the method by Su *et al.*²⁴ First, $\text{Bi}_4\text{Ti}_3\text{O}_{12}$ platelets were manufactured by reacting stoichiometric amounts of Bi_2O_3 and TiO_2 (both 99.9% , Sigma-Aldrich, St Louis, MO, USA) in an equimolar mixture of KCl and NaCl (both 99.997% , Alfa Aesar, Karlsruhe, Germany). A weight ratio of salt to reactants of 1:1 was used both in this and all the following molten salt processes. The mixture was reacted in an enclosed alumina crucible at $1100\text{ }^\circ\text{C}$ for 6 h using heating and cooling rates of $600\text{ }^\circ\text{C/h}$. The product was washed with hot distilled water, filtered and dried. Conversion to BaTiO_3 was performed with addition of BaCO_3 (mol BaCO_3 : mol $\text{Bi}_4\text{Ti}_3\text{O}_{12}$ of 1) in an equimolar mixture of KCl and NaCl at $1040\text{ }^\circ\text{C}$ for 3 h using heating and cooling rates of $600\text{ }^\circ\text{C/h}$. The product mixture (BaTiO_3 and Bi_2O_3) was

separated from the salt flux by washing with hot distilled water, then filtered and dried. Next, the products were washed with hot 6 M HNO₃ to dissolve Bi₂O₃ and unreacted BaCO₃, then filtered and dried. In the final step, washing with hot distilled water, filtering and drying was performed to dissolve Ba(NO₃)₂ and obtain the target phase BaTiO₃.

(111)-oriented BaTiO₃ platelet templates were also manufactured by molten salt synthesis and conversion, based on the method by Sato *et al.*²⁵ First, Ba₆Ti₁₇O₄₀ was synthesized by reacting TiO₂ (anatase) (99.8 %, Sigma-Aldrich, St Louis, MO, USA) with excess BaTiO₃ (99 %, Sigma Aldrich, St Louis, MO, USA) (BaTiO₃:TiO₂ of 6:9) in NaCl. The mixture was placed in an enclosed platinum crucible, heated to 800 °C (1 h dwell) and then to 1150 °C (1 h dwell) using heating and cooling rates of 200 °C/h. The product was washed with hot distilled water, filtered and dried. BaTiO₃ was synthesized by mixing stoichiometric quantities of Ba₆Ti₁₇O₄₀ and BaCO₃ in NaCl. The mixture was reacted and washed in an identical manner as for the synthesis of Ba₆Ti₁₇O₄₀.

Both <100>-, <111>- and non-textured BCT ceramics were manufactured by tape casting and templated grain growth. Aqueous slurries for tape casting were prepared according to the method by Lein *et al.*^{14,26} The dry content of the slurries consisted of 90 wt% BCT matrix powder and 10 wt % BaTiO₃ templates, (100)- or (111)-oriented. BaTiO₃ isometric powder of ~0.7 μm particle size (99 %, Sigma Aldrich, St Louis, MO, USA) was used instead of templates for synthesis of template-free tapes and non-textured ceramics. The slurries were tape cast by a Mistler Table Top Caster (TTC-1200, Richard E. Mistler, Inc., Morrisville, PA) on a Mylar™ film at a speed of 60 cm/min. After drying for ~20 h at ambient conditions, green tape cut-outs were stacked and laminated. Green compacts for conventional sintering were laminated by hot pressing at 30 MPa for 10 min at 80 °C. Some compacts consisted of

alternating tapes with templates ((100)- or (111)-oriented) and template-free tapes, reducing the overall template loading to 5 wt% as an attempt at avoiding delamination and pores between the tape layers. All green compacts were subjected to binder-burnout at 600 °C for 6 h (heating rates of 25 °C/h to 180 °C, 12 °C/h further up to 600 °C). Conventional sintering was performed at 1450 °C in air with a heating rate of 200 °C/h.

Spark plasma sintering (SPS) was used as another approach to avoid delamination and increase the density of the BCT laminates. Compacts for SPS were fabricated by wetting each tape cut-out with water prior to stacking and reducing the lamination time to < 2 min, the temperature to 70 °C and the pressure to < 15 MPa. SPS was performed under vacuum using a Dr Sinter 2050 SPS (Sumitomo Coal Mining Co., Tokyo, Japan). The inside of the graphite die (12 mm inner diameter) was covered with graphite sheets. The laminated samples were placed in a powder bed of ~1 g BCT powder, with Pt sheets between the samples and the powder bed to protect the samples. SPS was performed by applying a constant heating rate of 100 °C/min up to 1000 °C, followed by 50 °C/min up to a hold temperature of 1250 °C. The dwell time at the maximum temperature was 5 min. The application of pressure started at 1000 °C, where the load was manually increased up to a pressure of 50 MPa when the maximum temperature was reached. All the SPS samples were subsequently sintered at 1450 °C for 10 h, (i.e. the same as the conventionally prepared laminates) to ensure sufficient development of texture through the templated grain growth process. All samples used in this work are presented in Table I and assigned a sample code which includes the type of texture, the number of the parallel and if they were prepared using SPS.

The density of the sintered ceramics was measured by the Archimedes' method in isopropanol (ISO 5017). X-ray diffraction (XRD) patterns were recorded for powders, templates and

sintered ceramics (D8 Focus, Bruker AXS, Karlsruhe), and Lotgering factors²⁷ (F) quantifying the degree of <100> or <111> texture were calculated from the relative intensities (not integrated areas) of the Bragg reflections using the non-textured sintered ceramics as the reference. The temperature dependence of the crystal structure of BCT was investigated from -165 to 140 °C in 5 °C steps (D8 Advance, Bruker AXS, Karlsruhe, Germany, Cu K α radiation) with a MRI TC-Wide Range camera. The powder for this analysis was obtained by crushing and annealing a ceramic sintered at 1350 °C. Scanning electron microscopy (SEM) was used to investigate microstructure and morphology (S-3400N, Hitachi, Hitachi, Japan). Piezo- and ferroelectric properties were investigated with a TF Analyzer 2000 (aixACCT Systems GmbH, Aachen, Germany) at a frequency of 0.25 Hz and a triangular waveform. The electric field-induced strain amplitude, S_{\max} , and the corresponding strain coefficient, S_{\max}/E_{\max} , were measured through the application of unipolar electric field cycles. The piezoelectric coefficient d_{33}^* was measured with a d_{33} -meter (90-2030, APC Products Inc, Mackeyville, PA, USA).

Results

Phase-pure (by XRD, Fig. 1) BCT powder consisting of $\sim 0.5 \mu\text{m}$ isometric particles (Fig. 2(a)) was successfully manufactured by solid state synthesis. The stability of the tetragonal ($P4mm$) polymorph of BCT between $\sim -40^\circ\text{C}$ and $\sim 130^\circ\text{C}$ was confirmed by non-ambient XRD. The XRD patterns are shown in the supplementary information²⁸ (Fig. S1). The two-step molten salt method was demonstrated to be suitable for the synthesis of BaTiO₃ templates with platelet morphology (Figs. 2(b) and (c)). The crystallographic orientation of the two kinds of platelets (either (100) or (111)) was demonstrated by the enhancement of ($h00$) or (111) diffraction lines (Fig. 1).

Textured ceramics with F up to 99 % for $\langle 100 \rangle$ texture and 84 % for $\langle 111 \rangle$ texture were obtained by tape casting and templated grain growth (Fig. 3 and Table I). The densities of conventionally sintered textured ceramics were all < 93 %. Scanning electron microscopy revealed a microstructure consisting of isometric grains of about 50 μm in size as displayed in Fig. 4(a). Some porosity, originating from insufficient lamination of the stacked tapes, was observed by electron microscopy. This particular porosity lowered the overall density of the laminated, textured ceramics. These pores were not observed in the non-textured ceramics. Inclusion of a template-free tape between each template-containing (samples 100#2 and 111#2) slightly increased the density, and improved the degree of $\langle 111 \rangle$ texture (Table I). With a modified lamination procedure and SPS the density increased to > 96 % and no delamination was observed (Table I and Fig. 4(b)). No improvement in the degree of texture was obtained with SPS (Table I).

Polarization-electric field and strain-electric field loops displayed in Fig. 5 demonstrate enhanced and reduced bipolar strain in the $\langle 100 \rangle$ - and $\langle 111 \rangle$ -textured materials, respectively, relative to the non-textured BCT. The $\langle 100 \rangle$ -textured BCT prepared by SPS reaches bipolar strain up to 0.1 %. There is no significant variation in the spontaneous or remanent polarization, or the coercive field between the different sample types. The significantly increased piezoelectric response obtained by $\langle 100 \rangle$ texture and decreased response with $\langle 111 \rangle$ texture is further demonstrated by the unipolar strain upon electric field loading and the piezoelectric coefficient d_{33}^* (Fig. 6(a-b)). The data for the different materials are summarized in Table I. The $\langle 100 \rangle$ -textured SPS sample reaches a strain up to 621 pm/V and a d_{33}^* of 207 pC/N. In contrast, the highest corresponding values for the $\langle 111 \rangle$ -textured BCT are 234 pm/V and 113 pC/N, which are lower than for non-textured BCT (336 pm/V and 155 pC/N). Moreover, Fig. 6(c) shows that the $\langle 100 \rangle$ -textured BCT possess higher

performance than $\langle 111 \rangle$ - and non-textured BCT in the entire temperature region examined in this work (25-125 °C). The $\langle 100 \rangle$ -textured BCT exhibits a stable strain response upon heating until the temperature reaches 100 °C, while the non-textured, and to a certain degree the $\langle 111 \rangle$ -textured, display an initial decrease in the strain values when the temperature is raised above 25 °C.

Discussion

The merit of this study of textured BCT ceramics is twofold. Firstly, we demonstrate that high and temperature-stable properties are attainable with $\langle 100 \rangle$ texturing in a new lead-free system. Both the values of bipolar and unipolar strain and d_{33}^* of $\langle 100 \rangle$ -textured BCT are higher than the corresponding values for $\langle 111 \rangle$ - and non-textured ceramics. Piezoelectric coefficients above 200 pC/N and strain of 0.1 % and 621 pm/V are in the upper range of reported lead-free ferroelectrics.^{29,30} Thus the temperature stable strain in the chosen BCT composition up to 100 °C in combination with the enhanced piezoelectric performance along the polar direction make the $\langle 100 \rangle$ -textured BCT ceramics promising for actuator applications. Secondly, we have demonstrated the importance of the crystallographic direction of the texture. While increased performance for $\langle 100 \rangle$ textured ceramics is observed, the response decreases for $\langle 111 \rangle$ textured BCT, also compared to non-textured ceramics. This leads to two important conclusions: (i) applying the electric field parallel to the polar axis ($[100]$) in BCT is beneficial compared to parallel a non-polar axis ($[111]$), and (ii) the anisotropy of the intrinsic piezoelectric effect dominates over any extrinsic effect due to aligned grains in any crystallographic direction.

Piezoelectric enhancement in $\langle 100 \rangle$ -textured BCT demonstrates that this material is an extender ferroelectric; this is further rationalized in the following. Since the rotator/extender properties are dependent on the piezoelectric coefficients (Equation 1), their variation with temperature induces a temperature dependence on the direction of maximum intrinsic piezoelectric response. Because a complete set of piezoelectric coefficients are not readily available for most compositionally engineered piezoelectric systems, well-known materials such as BaTiO_3 may therefore serve as a compositionally and structurally comparable prototype for our considerations. The piezoelectric coefficients of BaTiO_3 as a function of temperature are shown in Fig. 7. The coefficients are strongly temperature dependent for each polymorph, and change across the phase transitions. For example is $d_{15} > d_{33}$ around room temperature and $d_{33} > d_{15}$ close to T_C . This temperature variation originates from change of symmetry, more specifically a relaxation of the dielectric susceptibility in certain directions at the phase transition temperatures.³¹ The consequence of the T-O phase transition in BaTiO_3 and its effect on d_{33}/d_{15} is a change from rotator-type ferroelectricity at room temperature to extender-type at higher temperatures up to T_C . For example PbTiO_3 which does not have a T-O transition is an extender within the entire temperature range.⁶ Consequently, suppressing the T_{T-O} in BCT relative to BaTiO_3 should also suppress the rotator ferroelectric range, meaning that BCT should display extender ferroelectricity from room temperature to the T_C . This was indeed observed in this work. Similar reasoning is expected to be applicable for other material systems.

In addition to increasing the piezoelectric response by utilizing the extender ferroelectricity of BCT, the $\langle 100 \rangle$ texture provides temperature stability of the properties. As shown in Fig. 6(c), the $\langle 100 \rangle$ -textured BCT display an almost temperature-independent strain up to temperatures close to T_C , in contrast to the $\langle 111 \rangle$ - and non-textured BCT. This can be

explained from Equation 1, which reduces to $d_{33}^* = d_{33}$ for perfect $\langle 100 \rangle$ texture (since $\theta = 0$). Consequently, the temperature dependence of $\langle 100 \rangle$ -textured BCT should equal that of d_{33} throughout the tetragonal range. For BaTiO_3 this coefficient increases monotonically at low temperatures and exponentially close to the T_C (Fig. 7); this thermal behavior is reproduced in data for $\langle 100 \rangle$ -textured BCT (Fig. 6(c)). The $\langle 111 \rangle$ - and non-textured BCT are dependent on not only d_{33} , but also d_{15} and d_{31} (since $\theta \neq 0$ in Equation 1), which induces a more complex thermal variation. For example, the slight enhancement of properties of $\langle 111 \rangle$ - and non-textured BCT when lowering the temperature from 50 to 25 °C in Fig. 6(c) displays the increasing contribution from d_{15} at lower temperatures. The temperature stability of $\langle 100 \rangle$ -textured BCT between room temperature and 100 °C is therefore primarily caused by the $\langle 100 \rangle$ texture, rather than the suppressed T_{T-O} .

A few challenges were encountered in the synthesis of the BaTiO_3 templates and the textured BCT ceramics. Since the low-energy planes of perovskites are assumed to be $\{100\}$,³² synthesis of (100)-oriented templates and textured ceramics is more straightforward than (111)-oriented. This is reflected in the higher degree of texture ($F = 99\%$) obtained for $\langle 100 \rangle$ compared to $\langle 111 \rangle$ ($F = 84\%$) in this work. The degree of $\langle 111 \rangle$ -texture obtained in BCT is still higher than previously reported for BaTiO_3 .²⁵ Densification challenges were encountered with the use of platelet templates, regardless of their crystallographic orientation. As observed from the porosity parallel to the direction between the tape layers in Fig. 4(a), the problem was related to poor lamination between individual tapes rather than sintering of the BCT matrix powder. The inclusion of template-free tapes to reduce the template loading yielded a modest improvement of the density, while modifying the lamination procedure and using SPS resulted in perfectly laminated samples with comparable density to non-textured BCT. The key to these improved properties is further optimization of the lamination procedure;

synthesis of dense, textured BCT should therefore be possible also without SPS. Acquiring very dense ceramics do, however not, appear crucial for the effect of the different textures. Independent of the density, <100>-textured samples displayed higher piezoelectric properties than non-textured and <111>-textured BCT. A plot of d_{33}^* and S_{\max}/E_{\max} vs. density is presented in the supplementary information²⁸ (Fig. S6).

Conclusions

$\text{Ba}_{0.92}\text{Ca}_{0.08}\text{TiO}_3$ (BCT) ceramics with grains oriented along either <100> or <111>, as well as non-textured ceramics, were manufactured using tape casting and templated grain growth. A high degree of texture was obtained for both crystallographic directions, quantified by Lotgering factors of 99 and 84 % for <100> and <111> texture, respectively. The piezoelectric response was strongly enhanced in <100> textured ceramics, with E_{\max}/S_{\max} reaching a value of 621 pm/V, bipolar strain up to 0.1 % and a d_{33}^* -value of 207 pC/N. This high response was also stable up to 100 °C. <111>-textured BCT exhibited lower piezoelectric response compared to both <100>- and non-textured BCT. The results are in correlation with extender ferroelectricity in BCT, since the piezoelectric response was improved parallel to the polar axis and reduced parallel to a non-polar axis. Such response was also predicted based on the thermal variations in the piezoelectric coefficients of BaTiO_3 . This demonstrates that considerations of the piezoelectric anisotropy and rotator/extender ferroelectricity are necessary when using texture to optimize lead-free piezoelectrics.

Acknowledgements

The authors thank MSc Dehlia Eide Brennhaugen for performing initial studies on the BCT system and Dr. Julian Tolchard for collecting the temperature dependent XRD data. Financial support from NTNU and the Research Council of Norway through project number 197497/F20 «Lead-free ferro- and piezoelectric $K_{0.5}Na_{0.5}NbO_3$ -based materials» is acknowledged.

References

- 1 J. L. Jones, B. J. Iverson, and K. J. Bowman, *J. Am. Ceram. Soc.* **90**, 2297 (2007).
- 2 G. L. Messing, S. Trolier-McKinstry, E. M. Sabolsky, C. Duran, S. Kwon, B. Brahmaroutu, P. Park, H. Yilmaz, P. W. Rehrig, K. B. Eitel, E. Suvaci, M. Seabaugh, and K. S. Oh, *Crit. Rev. Solid State Mat. Sci.* **29**, 45 (2004).
- 3 D. Damjanovic, *J. Am. Ceram. Soc.* **88**, 2663 (2005).
- 4 M. Davis, M. Budimir, D. Damjanovic, and N. Setter, *J. Appl. Phys.* **101**, 054112 (2007).
- 5 M. Davis, PhD Thesis, EPFL, 2006.
- 6 D. Damjanovic, M. Budimir, M. Davis, and N. Setter, *J. Mater. Sci.* **41**, 65 (2006).
- 7 S. Wada, T. Muraishi, K. Yokoh, K. Yako, H. Kamemoto, and T. Tsurumi, *Ferroelectrics* **355**, 37 (2007).
- 8 S.-E. Park, S. Wada, L. E. Cross, and T. R. Shrout, *J. Appl. Phys.* **86**, 2746 (1999).
- 9 Z. Yu, R. Guo, and A. S. Bhalla, *Appl. Phys. Lett.* **77**, 1535 (2000).
- 10 Z. Yu, R. Guo, and A. S. Bhalla, *Materials Letters* **57**, 349 (2002).
- 11 S. Wada, A. Seike, and T. Tsurumi, *Jpn. J. Appl. Phys.* **1** **40**, 5690 (2001).
- 12 A. Pramanick, D. Damjanovic, J. E. Daniels, J. C. Nino, and J. L. Jones, *J. Am. Ceram. Soc.* **94**, 293 (2011).
- 13 Y. Saito, H. Takao, T. Tani, T. Nonoyama, K. Takatori, T. Homma, T. Nagaya, and M. Nakamura, *Nature* **432**, 84 (2004).
- 14 A. B. Haugen, G. H. Olsen, F. M. Madaro, M. I. Morozov, G. Tutuncu, J. L. Jones, T. Grande, and M. A. Einarsrud, Accepted.
- 15 W. Liu and X. Ren, *Phys. Rev. Lett.* **103**, 257602 (2009).
- 16 S. K. Ye, J. Y. H. Fuh, and L. Lu, *Appl. Phys. Lett.* **100** (2012).
- 17 J. Hao, W. Bai, W. Li, and J. Zhai, *J. Am. Ceram. Soc.* **95**, 1998 (2012).
- 18 Y. Cui, X. Liu, M. Jiang, Y. Hu, Q. Su, and H. Wang, *J Mater Sci: Mater Electron* **23**, 1342 (2012).
- 19 D. S. Keeble, F. Benabdallah, P. A. Thomas, M. Maglione, and J. Kreisel, *Appl. Phys. Lett.* **102** (2013).
- 20 A. B. Haugen, J. S. Forrester, D. Damjanovic, B. Li, K. J. Bowman, and J. L. Jones, *J. Appl. Phys.* **113**, 014103 (2013).
- 21 J. Gao, D. Xue, Y. Wang, D. Wang, L. Zhang, H. Wu, S. Guo, H. Bao, C. Zhou, W. Liu, S. Hou, G. Xiao, and X. Ren, *Appl. Phys. Lett.* **99**, 092901 (2011).
- 22 B. Jaffe, W. R. Cook, and H. Jaffe, *Piezoelectric Ceramics* (Academic Press Inc., London, 1971).
- 23 T. Mitsui and W. B. Westphal, *Physical Review* **124**, 1354 (1961).

- ²⁴ S. Su, R. Zuo, D. Lv, and J. Fu, *Powder Technology* **217**, 11 (2012).
- ²⁵ T. Sato and T. Kimura, *Ceram. Int.* **34**, 757 (2008).
- ²⁶ H. L. Lein, T. Tezuka, T. Grande, and M.-A. Einarsrud, *Solid State Ion.* **179**, 1146 (2008).
- ²⁷ F. Lotgering, *J. Inorg. Nucl. Chem.* **9**, 113 (1959).
- ²⁸ See supplementary information at [] for more detailed results.
- ²⁹ J. Rödel, W. Jo, K. T. P. Seifert, E. M. Anton, T. Granzow, and D. Damjanovic, *J. Am. Ceram. Soc.* **92**, 1153 (2009).
- ³⁰ W. Jo, R. Dittmer, M. Acosta, J. Zang, C. Groh, E. Sapper, K. Wang, and J. Rödel, *J. Electroceram.* **29**, 71 (2012).
- ³¹ D. Damjanovic, F. Brem, and N. Setter, *Appl. Phys. Lett.* **80**, 652 (2002).
- ³² T. Sano, D. M. Saylor, and G. S. Rohrer, *J. Am. Ceram. Soc.* **86**, 1933 (2003).

Table

Table I. BCT samples (<100>, <111>- and non-textured) and their density (ρ), Lotgering factor (F), normalized strain (S_{\max}/E_{\max}) and piezoelectric coefficient (d_{33}^*). Samples 100#2 and 111#2 were laminated by including a template-free tape between each templated tape and therefore contain only 5 wt% templates.

Sample code	ρ (%)	F (%)	S_{\max}/E_{\max} (pm/V)	d_{33}^* (pC/N)
100#1	90	99	400 \pm 3	149 \pm 1
100#2	92	98	507 \pm 1	191 \pm 2
100SPS	96	97	621 \pm 3	207 \pm 3
111#1	87	76	206 \pm 2	92 \pm 8
111#2	89	84	198 \pm 7	97 \pm 1
111SPS	98	67	234 \pm 4	113 \pm 3
non-tex#1	97	-	332 \pm 5	150 \pm 1
non-tex#2	97	-	325 \pm 12	155 \pm 2
non-texSPS	96	-	336 \pm 1	142 \pm 5

Figures

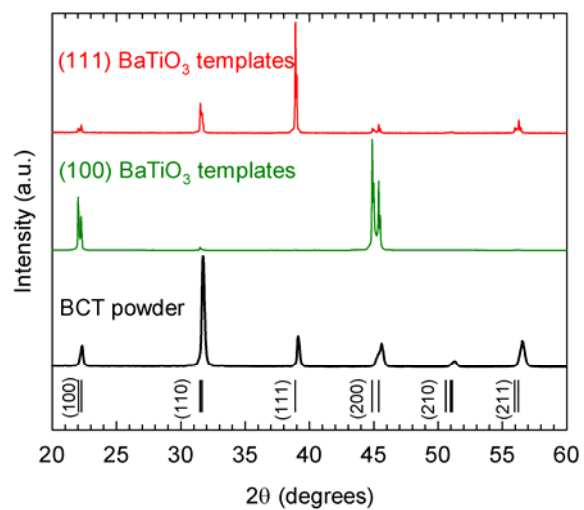


Fig. 1. XRD of BCT powder, (100)- and (111)-oriented BaTiO₃ platelet templates. Each diffractogram is normalized on its most intense reflection. Diffraction lines for tetragonal ($P4mm$) BaTiO₃ (PDF 00-005-0626) are included as a reference.

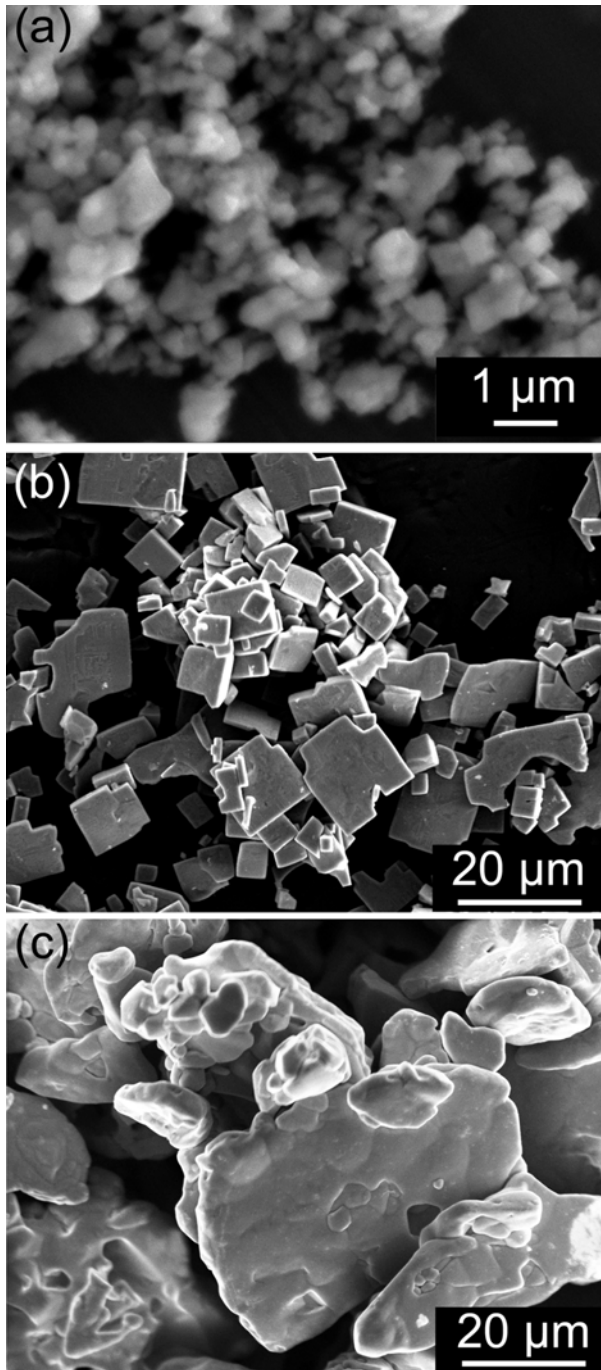


Fig. 2. SEM images of (a) BCT powder, (b) (100)-oriented BaTiO₃ templates and (c) (111)-oriented BaTiO₃ templates, all prior to tape casting.

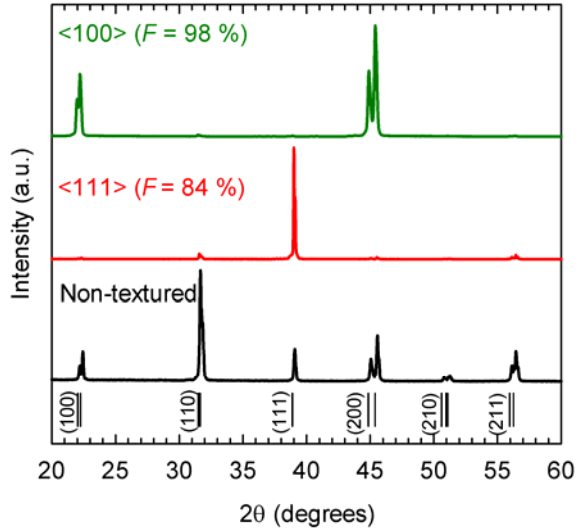


Fig. 3. XRD patterns of <100>- , <111>-textured and non-textured BCT ceramics manufactured by tape casting and templated grain growth. Lotgering factors are included in parentheses. Diffraction lines for tetragonal ($P4mm$) BaTiO_3 (PDF 00-005-0626) are included as a reference.

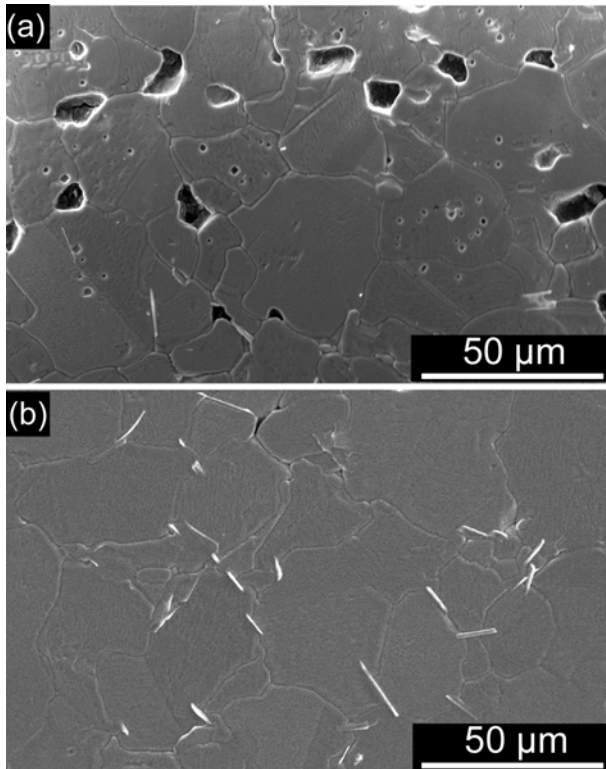


Fig.4. SEM images of cross-sections of $\langle 100 \rangle$ -textured BCT after (a) conventional sintering (90 % dense) and (b) spark plasma sintering (96 % dense). The tape casting plane is horizontal in the images. More SEM images of sintered BCT are available in the supplementary information²⁸, Figs. S2 and S3.

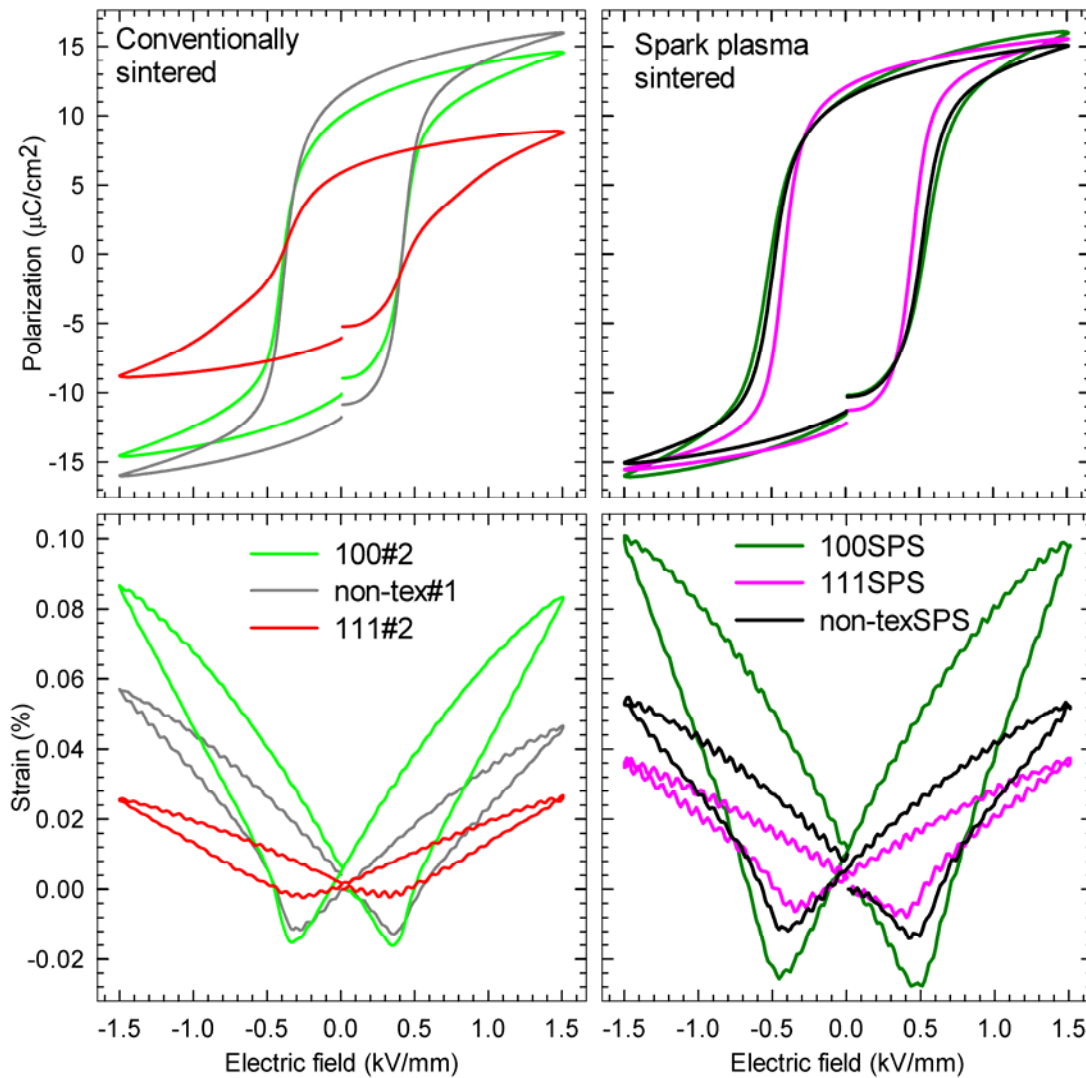


Fig. 5. Polarization and strain vs. electric field of $\langle 100 \rangle$ -, $\langle 111 \rangle$ -textured and non-textured BCT samples. The panels to the left show conventionally sintered samples while the panels to the right show spark plasma sintered samples. More samples are included in Fig. S4 in the supplementary information²⁸.

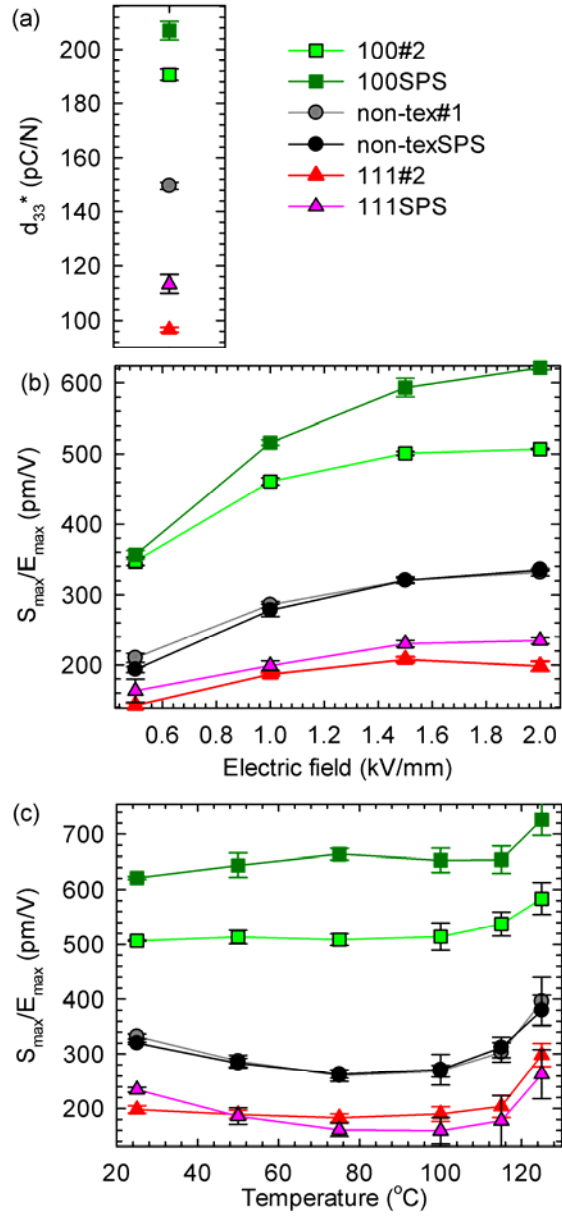


Fig. 6. (a) d_{33}^* , (b) S_{max}/E_{max} and (c) S_{max}/E_{max} (at 2 kV/mm) vs. temperature of BCT samples with different types of texture. More samples are included in Fig. S5 in the supplementary information²⁸.

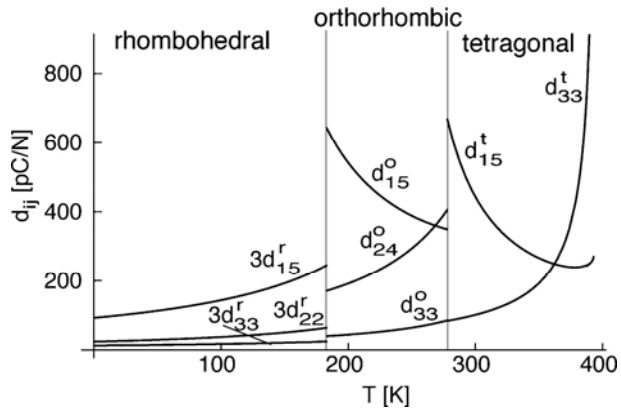


Fig. 7. Piezoelectric coefficients of BaTiO₃ in its ferroelectric phases predicted by theory.

Reprinted with permission from Damjanovic *et al.* (ref. ⁶).